Targeting the unstable atherosclerotic plaque : diagnostic and therapeutic implications

Segers, F.M.E.

Chapter 2

Identification of a Novel Peptide Antagonist of SR-AI as Atherosclerosis-targeted Imaging Agent

Filip M.E. Segers*[1], Haixiang Yu*[1], Tom J.M. Molenaar[1], Perry Prince[1], Sandra van Heiningen, Toshiki Tanaka[2], Theo J.C. van Berkel[1], and Erik A.L. Biessen[1,3]

(*Both authors contributed equally)

[1] Division of Biopharmaceutics, Leiden/Amsterdam Center for Drug Research, Leiden University, Leiden, The Netherlands
[2] Department of Material Science, Graduate School of Engineering, Nagoya Institute of Technology, Nagoya, Japan
[3] Department of Pathology, Cardiovascular Research Institute Maastricht, Maastricht University, Maastricht, The Netherlands

(Submitted for publication)

Abstract

Background - Scavenger receptor A (SR-A) is abundantly expressed by macrophage and plays a critical role in foam cell formation and atherogenesis. In search of selective SR-AI antagonists, we have employed affinity selection of a phage displayed peptide library on a synthetic receptor comprising the ligand binding site.

Methods and Results - Phage selection led to an almost 1,000 fold enrichment of SR-AI binding phage, which bound avidly to human THP-1 and moderately to murine RAW264.7 macrophages. Phage binding could be displaced by polyinosinic acid and succinylated human serum albumin. A 15-mer corresponding to the peptide insert of the major SR-AI binding phage (PP1) displaced phage binding to SR-AI at an IC^{50} of 29mmol/L. The minimal essential motif required for SR-AI interaction was defined. After docking to a streptavidin scaffold, peptides were effectively internalized by macrophages in an SR-AI dependent manner. The enriched phage pool and streptavidin immobilized PP1 exhibited a similar in vivo biodistribution profile in mice with marked accumulation in hepatic macrophages. Importantly, PP1 docking onto ^{125}I-streptavidin increased its uptake by advanced aortic plaques of $ApoE^{-/-}$ mice more than 2-fold.

Conclusions - We have identified a novel peptide antagonist selective for SR-AI, which proved effective in SR-AI targeted imaging of atherosclerotic lesions.

Introduction

Macrophages play a key role in atherosclerosis at all stages of disease development[1]. They express a range of scavenger receptors such as scavenger receptor A (SR-A)[2-5] which are widely regarded as the driving force in foam cell formation by mediating the uptake of modified low density lipoproteins (LDL). SR-A is a trimeric transmembrane glycoprotein consisting of 6 distinct domains[2,6] and can exist in one of three isoforms (SR-AI, SR-AII and SRA-III)[7,8]. A pattern recognition receptor, it displays a very broad substrate profile, internalizing modified LDL, polynucleotides (e.g. polyinosinic and polyguanylic acid), polysaccharides (e.g. fucoidan) and lipopolysaccharides (LPS) [9-11]. SR-A is mainly expressed by resident macrophages but also by liver endothelial cells[12]. SR-A was found to be abundantly expressed by macrophages, foam cells and smooth muscle cells[13] in atherosclerotic lesions but not in the normal vessel wall[14,15]. The involvement of SR-A in atherogenesis was first established by Suzuki *et al*[4] showing that lesion formation was sharply reduced in SR-A-deficient ApoE$^{-/-}$ compared to ApoE $^{-/-}$ control mice. Subsequent studies were in support of this notion[16].

The marked expression of SR-AI in macrophage enriched sites of inflammation such as the atherosclerotic plaque and the fact that this receptor mediates the efficient endocytosis of its substrates indicates that SR-AI may not only be an interesting target for therapeutic intervention in atherosclerosis and inflammation but also for targeted drug delivery and imaging approaches[17]. Importantly, SR-AI expression is associated with newly invaded macrophages in the atheroma, which are particularly prominent in vulnerable plaque[18]. Application of selective SR-AI ligands as homing device for contrast agents may therefore not only improve the sensitivity of atherosclerotic plaque imaging but also may give insight into the actual composition and stability of the plaque.

Given the bulky and chemically complex nature of the macromolecular substrates for SR-AI it is not surprising that ligand design for this receptor has not been very successful and has only resulted in a single report on a synthetic, moderately selective SR-A antagonist[19]. In this study, we describe the unbiased design of SR-AI antagonists involving the use of phage display on a synthetic receptor comprising the actual ligand-binding pocket of SR-AI. A selective peptide antagonist for SR-AI was identified, which constitutes a promising lead to the development of SR-AI targeted therapy and imaging of atherosclerotic lesions.

MATERIALS AND METHODS

Phage library

The pComb3 phage displayed peptide library X_{15} (in which X is any amino acid) was generated by Dr Pannekoek and co-workers (University of Amsterdam, the Netherlands).

Peptide synthesis

All peptides were synthesized on an automated peptide synthesizer (9050 Millipore, MA) using standard Fmoc solid-phase peptide synthesis. Crude peptides were purified on a preparative C_8 RP-HPLC column (Altech, Deerfield, IL) using a JASCO PU-980 (Tokyo, Japan). Purified peptides were further characterized by LC-MS in Division of Analytical Biosciences, Leiden University. The purity of the peptide, as checked by MALDI-TOF mass spectrometry and RP-HPLC, was at least 70%. Biotinylated PP1 peptide LSLERFLRCWSDAPAK-biotin (BioPP1) was more than 95% pure. Lyophilized peptides were stored at -20°C under nitrogen until further use. Synthetic biotinylated bovine SR-AI was synthesized, purified and characterised as described by Suzuki et al[20].

Selection of SR-AI binding phage

10μg/mL of streptavidin in coating buffer (50mmol/L $NaHCO_3$, pH 9.6) was incubated overnight at 4°C in a high binding 96 well plate (Costar, Corning, UK) at 100μL/well. Subsequently, wells were washed with assay buffer (20 mmol/L HEPES, 150mmol/L NaCl, 1mmol/L $CaCl_2$, pH 7.4) and incubated for 1h at 37°C with blocking buffer (3% BSA in assay buffer). After washing, wells were incubated with 50μmol/L of biotinylated SR-AI (2h 37°C), washed, and subsequently incubated for 2 h at room temperature (RT) with the phage libraries at 10^9 colony forming units (CFU) in 100μL of binding buffer (0.1% BSA, 0.5% Tween 20 in assay buffer). Wells were washed 10x with binding buffer and binding phage were eluted by incubation for 5 min at RT with 100μL of elution buffer (0.1mol/L glycine/HCl, pH2.2) and neutralized by addition of 50μL of neutralization buffer (1mol/L Tris/HCl, pH8.5). Phage were titrated, amplified and purified as described[21]. Amplified phage was used for further selection. For DNA sequencing of enriched phage pools, plasmid DNA was isolated from single colonies using the Wizard plus SV Miniprep DNA Purification System (Promega, Madison, USA). DNA sequencing was conducted at the DNA-sequencing facility of the Leiden University Medical Center using a standard M13 primer. Unless otherwise stated, the amplified phage pool of round 7 was used for further characterization experiments.

Cell culture

Murine macrophage cells (RAW264.7), African green monkey kidney COS-7 and human monocytic THP-1 cells were grown in Dulbecco's Modified Eagles's

Medium (DMEM) supplemented with 10% (v/v) heat-inactivated fetal bovine serum (FBS), 100U/mL penicillin, and 100mg/mL streptomycin. Bone marrow derived macrophages were isolated from C57BL/6 mice and cultured as described before[22]. Cell cultures were maintained at 37°C in humidified 95% air/5% CO_2.

Cell binding assay

COS-7 and RAW264.7 cells were grown to approximately 60~70% confluency in 12-wells plates, while non-adherent THP-1 cells were grown to $4 \cdot 10^5$cells/well. Cells were pre-incubated in DMEM+0.2% BSA, 2h at 37°C. SR-AI specific phage (round 7) was added at a titer of 10^8 CFU and incubated for 2h at 4°C. Non-selected phage library was used as a negative control. RAW and COS-7 cells were washed 10x with phosphate-buffered saline (PBS) and lysis buffer (500µL Reporter E397A, Promega, Madison, USA) was added. The THP-1 cell suspension was washed 10x with PBS, subsequently centrifuged for 5 min at 10,000rpm and the cell pellet was resuspended in PBS. Finally, cells were lysed by adding 500µL lysis buffer. Input samples were taken from the incubation medium immediately after addition of the phage and diluted 1:100 in 1x Tris Buffered Saline (TBS) in a total volume of 1mL. Output samples were taken from the cell lysate and diluted 1:10 or 1:100 (total volume: 500µL). The recovery of bound phage was calculated from the output to input ratio.

Competition experiment of SR-AI selected phage pool

In analogy to the phage selection conditions, streptavidin (10µg/mL in coating buffer) was incubated overnight at 4°C in a high-binding 96-well plate at 100µL/well. Wells were washed 3x with assay buffer and incubated for 1h at 37°C with blocking buffer. Next, wells were incubated for 2 h at 37°C with 125nmol/L biotinylated SR-AI binding peptide (100µL/well), washed 3x with binding buffer, after which SR-AI ligands or synthetic SR-AI peptides (full length or N-terminal truncations of 7, 9, 11, 13 amino acids) were added and the solution (100µL) was left to incubate for 2h at RT with the enriched phage pool (round 7) at 10^8 cfu. Wells were washed 10x with binding buffer, binding phage were eluted by incubation for 5min at RT with 100µL elution buffer, and neutralized with 50µL neutralization buffer (1mol/L Tris-HCl, pH8.5). Residual phage binding was calculated from the input-to-output ratio.

In vivo distribution of SR-AI selective phage pool

SR-AI specific PP1 phage and a non-selected control phage were radiolabeled as previously described[21] and injected at 10^9 CFU (~200,000 DPM) via the tail vein into anesthetized C57Bl/6 mice (20 weeks old male; n=6). After 30 min, mice were perfused for 2 min with DMEM at 10mL/min via a cannula inserted in the left ventricle. Organs were removed, weighed and organ homogenates were obtained by overnight incubation with 500µL Solvable (Packard bioscience, Groningen, the

Netherlands) and analyzed for associated ^{35}S radioactivity in a beta counter after adding 4.5mL Hi-ionic Fluor (Perkin-Elmer, Boston, USA)

PP1 docking to streptavidin

To monitor optimal occupation of the available biotin binding sites, streptavidin (Amersham, Little Chalfont, UK) was incubated for 30 min at room temperature with bioPP1 at the indicated molar ratio in the presence of an excess amount of ^{3}H labeled biotin (~200, 000 DPM; Amersham). The mixture was then chromatographed over a Sephadex G-50 medium (Amersham) column (5mL), eluting with PBS and 500 µL fractions were collected. Samples were analyzed for radioactivity on a beta-counter after adding 4.5mL Hi-ionic Fluor (Perkin-Elmer, Boston, USA).

PP1 peptide binding to macrophage SR-AI

Bone marrow derived macrophages were matured by incubation with 20 µg/mL oxidized LDL overnight in a 9cm petridish. Adherent cells were detached by adding 3mL 4mmol/L EDTA. Cells were collected, centrifuged and washed with ice-cold PBS (4°C). The resuspended cells were incubated at 37°C in the dark in complete DMEM with 40nmol/L of streptavidin-PE (strepPE), strepPE-bioPP1 or strepPE-bioPP1 premixed with 1mg/mL fucoidan (Sigma, St. Louis, USA). After incubation with DAPI working solution (Molecular Probes, USA) for 30 min at RT, cells were washed and cytospins (300 rpm, 5min) were performed, mounted to the coverslip with fluorescent mounting medium (DAKO, Denmark) and analyzed under fluorescent microscope.

Displacement studies of PP1 binding to RAW 264.7 cells

Freshly prepared 0.38nmol/L ^{125}I-strep-bioPP1 was incubated with murine RAW264.7 cells (400,000) for 1h at 37°C in a 12-well plate in the presence of fucoidan at the indicated concentrations. Cells were subsequently washed 3x with 1mL ice-cold TBS/0.2% BSA (bovine serum albumin, pH7.4), and 3x with 1mL ice cold TBS and then lysed in 500µL 0.1mol/L NaOH. The radioactivity of the cell lysate was measured in a gamma counter.

In vivo organ distribution studies

C57Bl/6 mice (n=6; male, 20 weeks) were injected intravenously via the tail vein with 0.38nmol/L freshly prepared [^{125}I]-strep-biotin or [^{125}I]-strep-bioPP1 in 100µL of 0.9% sodium chloride. After 1h, mice were sacrificed, exsanguinated. Organs were removed and weighed, and the radioactivity entrapped in blood samples and organs was counted in a gamma counter.

In vivo colocalization of PP1 uptake with macrophages

Biotinylated PP1 was docked on strepPE (0.40µmol/L) at a 5:1 ratio as described earlier, and was intravenously injected via the tail vein in a C57Bl/6 and CD36$^{-/-}$/SR-A$^{-/-}$ mice (n=2). Biotin docked strepPE was used as a control. Mice were sacrificed 1 h after injection, perfused via a left ventricle cannula with PBS and fixed with 4% formaldehyde. Cryosections (5µm) of liver and spleen were prepared. Immunostaining was performed using a F4/80 monoclonal mouse antibody (1:100, BMA Biomedicals, Augst, Switzerland), an Alexa 488 labelled goat anti-rat secondary Ab (1:50, Molecular Probes Inc., Eugene, Oregon) and nuclear DAPI staining (Serva Feinbiochemica, Heidelberg, Germany). Slides were mounted with Fluorescence Mounting Medium (DAKO Netherlands B.V., Heverlee, Belgium) and analyzed on a Bio-Rad Radiance 2100 MP confocal laser scanning system equipped with a Nikon Eclipse TE2000-U inverted fluorescence microscope.

Molecular imaging of atherosclerotic tissue by PP1 peptides

Aged ApoE$^{-/-}$ mice (> 65 weeks, male, weight 30±2g, fed a chow diet) with advanced atherosclerotic lesions were intravenously injected with ^{125}I-strep-biotin or ^{125}I-strep-bioPP1 (0.38nmol/L, n=3). Mice were sacrificed and fixed as mentioned above. The aorta was isolated, stained for lipids with Oil Red O via a routine protocol and subjected to autoradiography, exposing it to a phosphor screen at room temperature for one week. The signal intensity was quantified by ImageQuant software (Bio-Rad, USA), and results expressed as percentage of the signal obtained in the ^{125}I-strep-bioPP1 treatment group. Images of the oil red-O-stained aortas were analyzed by automated image analysis software and lesion size expressed as relative oil red O stained area to total aorta.

Statistical Analysis and animal handling ethics

C57Bl/6 mice were obtained from Charles River laboratories, Maastricht, The Netherlands. ApoE$^{-/-}$ and SR-AI$^{-/-}$/CD36$^{-/-}$ mice were obtained from the local animal breeding facility (Leiden, the Netherlands). All animal work was approved by the regulatory authorities of Leiden and complied with the Dutch government guidelines. Values are expressed as mean±SD. A two-tailed unpaired Student's t-test was used to compare individual groups. A level of $P<0.05$ was considered significant.

RESULTS

Selection of SR-AI binding phage

A 15-mer phage displayed peptide library was screened for SR-AI binding peptide ligands. To favor the selection of peptides binding to the actual binding pocket of SR-AI, biopanning was performed on wells coated with a streptavidin associated, biotinylated peptide scaffold encompassing the complete ligand binding motif of SR-AI[20]. In the first two rounds a non-stringent washing protocol with ice-cold binding buffer was used, while from round three onwards stringency was gradually increased by decreasing the coating density of synthetic SR-AI and by using a binding buffer of room temperature for washing. This led to a significant enrichment of binding phage in the 5th round, culminating in an almost 1,000 fold increase after 7 rounds of biopanning (figure 2.1A). Subsequent DNA sequence analysis of 10 phage clones from the 6th and 7th selection round revealed a 12-mer consensus motif. 8/10 phage clones from round 6 shared the peptide sequence LSLERFLRCWSDAPA (PP1) while 2/10 clones carried a highly homologous LSLERFLRCWSDSPR (PP2) insert. In the 7th round, only PP1 clones were detected, suggesting that PP1 phage was more effectively bound than PP2. Compared with the parental non-selected phage library, the enriched phage pool showed high binding to streptavidin immobilized SR-AI but only marginal binding to streptavidin immobilized biotin or to type-2 collagen S. There was no binding of the control phage to streptavidin immobilized SR-AI, confirming that binding of the selected phage pool implicated the SR-AI moiety (figure 2.1B).

Cell binding of the enriched phage pool

To verify whether the selected phage pool (PP1) was also able to bind to the full-length receptor on macrophages, we have tested the ability of the phage pool binding to human THP-1 and murine RAW 264.7 cells, which both were shown to display SR-AI expression. Compared to the parental phage library, the selected phage avidly bound to THP-1 (figure 2.1C) and to a lesser extent to RAW264.7 cells. Binding to the latter was >2-fold higher than that to monkey COS-7 cells, which are SR-AI deficient.

Competition assay of phage binding to SR-AI by established SR-AI inhibitors

To further characterize the specificity and affinity of the selected phage binding, displacement studies of phage binding to synthetic SR-AI by the established SR-AI inhibitors polyinosinic acid (poly-I) and succinylated HSA (sucHSA) were performed. Both poly-I and suc-HSA were able to dose-dependently compete for phage binding to SR-AI at an IC_{50} of 10.5 and 66µg/mL, respectively (figure 2.1D).

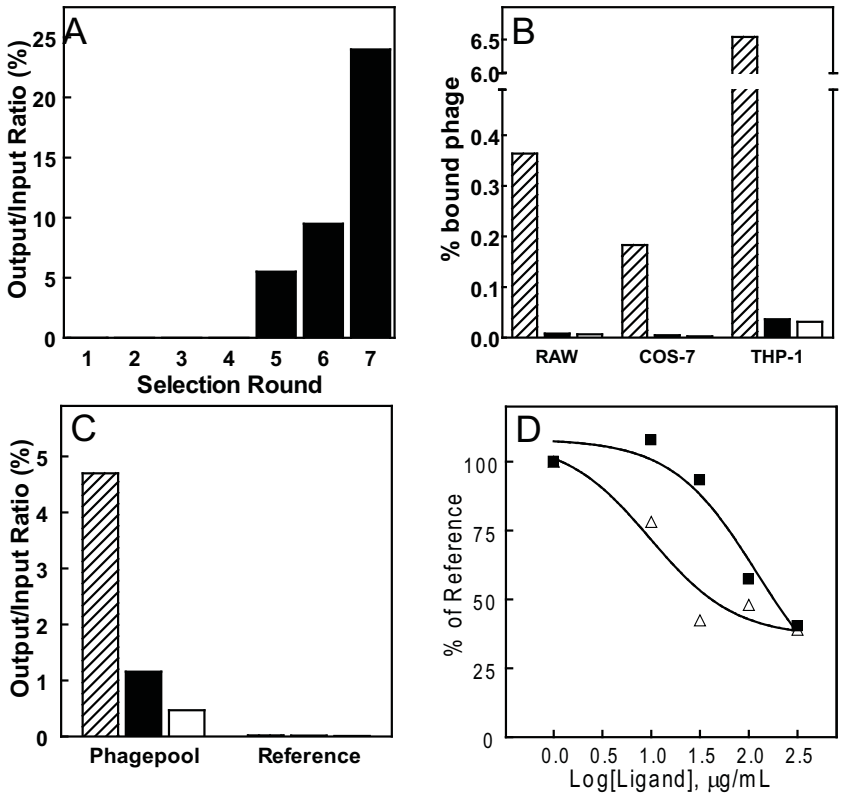

Figure 2.1 Selection and specificity of SR-AI binding phage. (A) Selection of the pComb3 X15 phage displayed peptide library on immobilized synthetic biotinylated SR-AI resulted in a sharp enrichment of SR-AI binding phage from the 5th round of selection onwards (up to 918-fold in the 7th round). (B) The enriched phage pool specifically bound to biotinylated SR-AI (hatched bars) but not to streptavidin immobilized biotin (black bars) or collagen S (open bars). As a reference, non-specific phage pool showed little binding to SR-AI. Values are expressed as output/input ratio and represent means of duplicate experiments. (C) Enriched phage pool (hatched bars) but not the parental library (WT; black bars) and the controlled nonspecific phage library (open bars) displayed avid binding to human THP-1 cells, moderate binding to murine RAW cells and poor binding to COS-7 cells. Values are expressed as output/input ratio and are means of two independent experiments. (D) Binding of the enriched phage pool to biotinylated SR-AI was determined in the presence of Suc-HSA (■) or poly I (Δ). IC_{50} values, as calculated from the competition curves were 66μg/mL and 10.5μg/mL, respectively. Values are expressed as percentage of total phage binding in the absence of the inhibitors and represent means of two independent experiments.

Competition assay of phage binding to SR-AI by synthetic peptides

DNA sequence analysis revealed the presence of a 12-mer consensus sequence within the peptide insert of the PP1/PP2 phage clones, suggesting the N-terminal part of the phage encoded peptide to be instrumental in SR-AI binding. To pinpoint the minimal peptide sequence required for SR-AI binding we have performed a truncation study, focusing mainly on the N-terminal of the peptide. Full-length peptide LSLERFLRCWSDAPA (PP1) and truncated peptides LERFLRCWSDAPA (PP1-13), RFLRCWSDAPA (PP1-11), LRCWSDAPA (PP1-9) and CWSDAPA (PP1-7) were synthesized by Fmoc chemistry. The capacity of the peptides to interfere

with phage binding to SR-AI was tested in a competition assay, at which residual binding of the selected phage to SR-AI was determined in the presence of the synthetic peptides (figure 2.2). PP1 could dose-dependently and potently inhibit SR-AI binding of the enriched phage at an IC_{50} value of 29μmol/L. Stepwise truncation of PP1 resulted in a gradual loss in affinity, and the 11-mer peptide PP1-11 was identified as the minimal motif of PP1 to be able to avidly bind SR-AI.

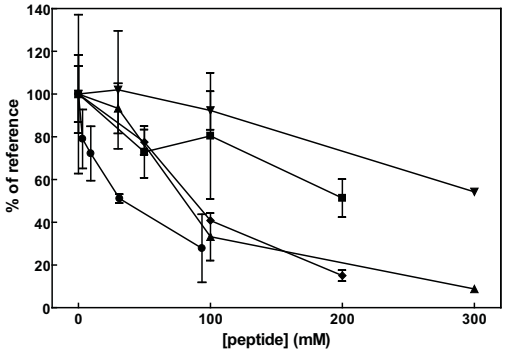

Figure 2.2 Competition of specific phage binding to SR-AI by synthetic PP1 peptide or trunctated analogues. Binding of the enriched phage pool to synthetic SR-AI was determined in the presence of 0~300 μmol/L of LSLERFLRCWSDAPA (●), LERFLRCWSDAPA (▲), RFLRCWSDAPA (♦), LRCWSDAPA (■), CWSDAPA (▼). Values are expressed as a percentage of total binding in the absence of peptide and represent means of three independent experiments ±SD. The IC50 values as calculated from the displacement curves were 29.1 μmol/L, 72.3 μmol/L, 80.9 μmol/L, 217 μmol/L and undetectable respectively.

PP1 peptide selectively binds to macrophage in a SR-AI dependent manner

We have incubated streptavidin with different molar ratio of biotinylated PP1 peptide to prepare tetrameric strep-bioPP1 complexes. Sephadex gel chromatography revealed that a protein to peptide ratio of 1:5 was optimal for conjugation and led to occupation of most of the biotin binding sites on streptavidin (figure 2.3A). Fucoidan, a polyanionic substrate of SR-AI, dose-dependently inhibited ^{125}I strep-bioPP1 binding to RAW264.7 at an IC50 of 4.2μmol/L (figure 2.3B).

To illustrate that strep-bioPP1 selectively binds to macrophages in a SR-AI dependent rather than non-specific manner, the binding of streptavidin-PE conjugated PP1 peptide to macrophages was investigated by immunocytochemistry. Bone marrow derived macrophages were cultured in conditioned medium containing macrophage colony-stimulating factor (M-CSF), to induce differentiation of progenitors into functional macrophages with SR-AI expression. FACS analysis was used to confirm the macrophage population (F4/80 positive>99%). When conjugated to the streptavidin scaffold, PP1 was able to confer significant uptake signal at concentrations as low as 40nmol/L. Furthermore, unlike strepPE-biotin, strepPE-bioPP1 specifically accumulated in macrophages (figure 2.3C). StrepPE-bioPP1 localized both at the membrane and in the cytosol, suggesting that PP1 uptake had occurred through receptor mediated rather than adsorptive endocytosis. Binding and internalization of strepPE-bioPP1 was abrogated by pretreatment with 1mg/mL fucoidan establishing once more underpinning the selectivity of PP1 for SR-AI.

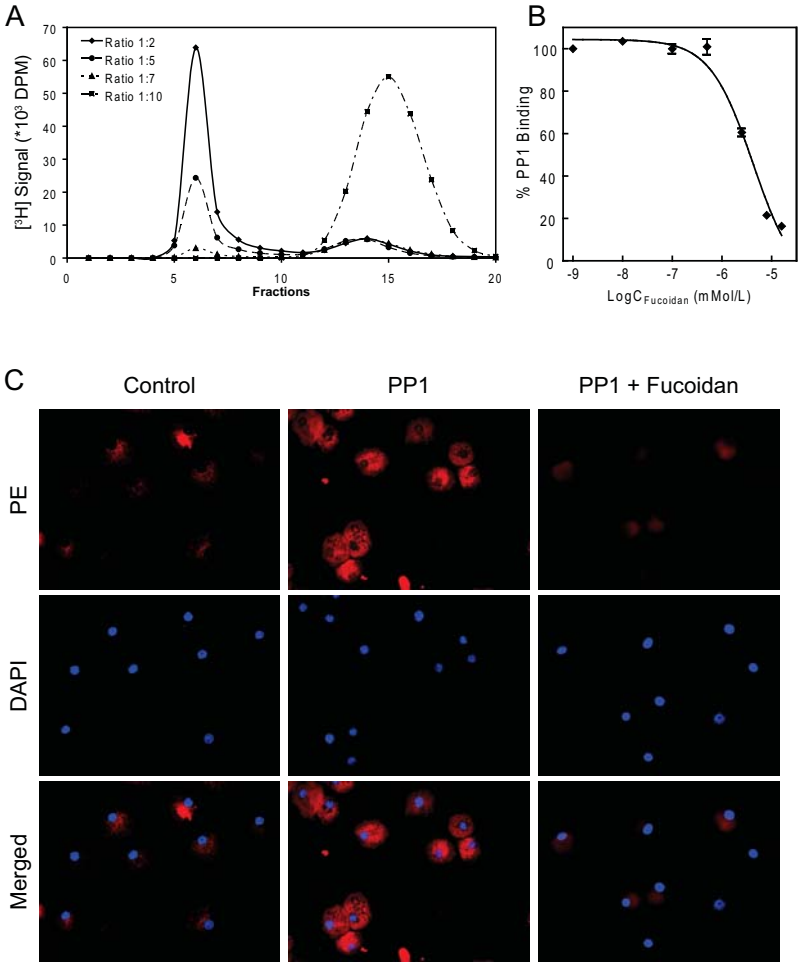

Figure 2.3 Streptavidin immobilized PP1 is internalized by macrophages in a SR-AI dependent fashion. (A) Sephadex gel chromatography was used to determine the optimal ratio of streptavidin to bioPP1 (B) ^{125}I strep-bioPP1 was incubated with murine macrophage RAW 264.7 cells in the presence of fucoidan at the indicated concentrations. The radioactivity of the bound radioligand was measured. Values represent means±SD of three individual experiments. (C) Bone marrow derived murine macrophages were incubated with strepPE-biotin, strepPE-bioPP1 or strepPE-bioPP1 pretreated with 1 mg/mL fucoidan. Representative microscopic views illustrate effective uptake of strepPE-PP1 (red) by macrophages which is prevented by pretreatment with fucoidan. Second and third rows show corresponding nuclear DAPI staining (blue) and DAPI/PE overlay, respectively.

Selective uptake of SR-AI binding phage and phage encoded peptide in vivo

As SR-AI is mainly expressed by resident macrophages in various organs including liver[23], we have examined the capacity of PP1 phage and PP1 peptide to accumulate in the liver after intravenous injection into C57Bl/6 mice. The PP1 phage displayed a significant 2-fold increase in liver accumulation compared to control phage. Liver and spleen appeared to be the most prominent sites of uptake, whereas less phage could be recovered from the heart (figure 2.4A). ^{125}I-streptavidin conjugated PP1 showed a similar biodistribution pattern with again a substantial 2-fold increased accumulation by liver (P=0.002), albeit that at an absolute level hepatic strep-bioPP1 uptake was less pronounced than that of PP1 phage (figure 2.4B).

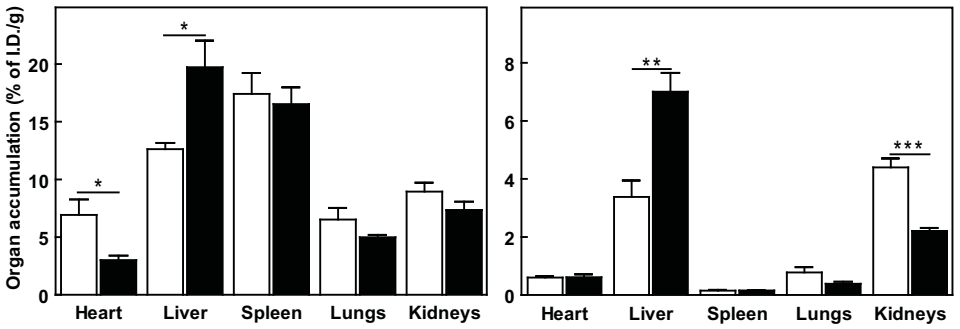

Figure 2.4 SR-AI binding phage as well as PP1 peptide home to SR-AI rich tissue in vivo. (A) [^{35}S]-labelled (200,000 DPM) SR-AI binding phage (black bars) and nonspecific control phage (open bars) were administered by tail vein injection to C57Bl/6 mice (n=6). After 30 min circulation, organs were harvested and the tissue distribution of radiolabelled phage was determined as percentage of the injected dose/g tissue. (B) ^{125}I strep-biotin (open bars) or ^{125}I strep-bioPP1 (black bars) was intravenously injected to C57Bl/6 mice (n=6). After circulating for 1h, organs were harvested and the tissue distribution of radioligand was calculated as a percentage of the injected dose/g tissue. Values represent means ±SD of three individual experiments. (*P<0.05, **: P<0.01).

As SR-AI and CD36 were found to be the major scavenger receptors responsible for ligand uptake[24], we intravenously (i.v.) injected strepPE labelled PP1 into C57Bl/6 and SR-AI$^{-/-}$/CD36$^{-/-}$ mice. StrepPE labelled biotin i.v. injected to C57Bl/6 mouse was used as a control. Immunofluorescent staining of macrophages (green) in spleen (figure 2.6) and in liver (figure 2.5) sections of C57Bl/6 mouse showed clear peptide accumulation and consistent colocalization of F4/80 positive macrophages with strepPE-PP1 (red) but not with biotin conjugated PE signal. Importantly, PP1 targeted strepPE was barely detectable in macrophage-rich tissue of SR-AI$^{-/-}$/CD36$^{-/-}$ mice. Taken together, we demonstrated that PP1 induced spleen and liver uptake was attributable to macrophages and mediated by scavenger receptors.

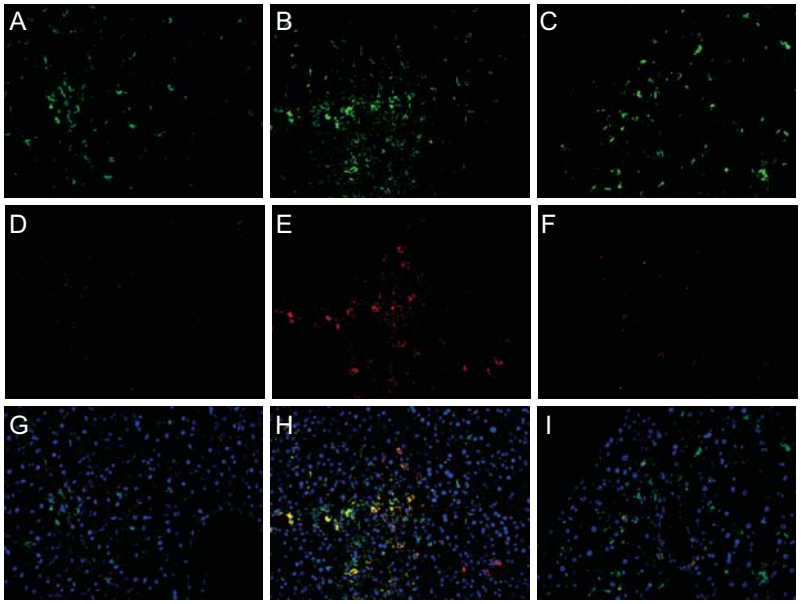

Figure 2.5 Streptavidin-PE docked PP1 colocalizes with liver macrophages in a scavenger receptor dependent manner. Streptavidin PE conjugated PP1 was administered by tail vein injection to C57Bl/6 (B, E, H) or SR-A$^{-/-}$CD36$^{-/-}$ mice (C, F, I, n=2). Mice were sacrificed and organs were harvested 1h after injection. StrepPE-biotin injected to C57Bl/6 mouse was used as a control (A, D, G). Representative merged photomicrographs of liver cryosections stained for the presence of mouse macrophages by F4/80 (green), PP1 conjugate uptake by PE fluorescence (red) and nuclei by DAPI (blue) were given respectively. Colocalization of macrophage with PP1 is yellow (Magnification 20x).

PP1 peptide targets atherosclerotic aortic artery lesions in ApoE$^{-/-}$ mice

Since SR-AI was found to be considerably overexpressed in atherosclerotic lesions, we finally examined the capacity of PP1 peptide to target carriers to aortic artery lesions in aged ApoE$^{-/-}$ mice. Lesion size was expressed as relative Oil Red O stained aortic area and amounted approximately 50% (figure 2.6), reflecting the advanced stage of lesion development at 16 months. Importantly, although the plaque size in both treated groups did not differ, accumulation of radioactivity in aortas after ^{125}I strep-bioPP1 injection was two-fold higher than that after injection of ^{125}I strep-biotin (P=0.007). We conclude that PP1 facilitates the targeting of carriers to atherosclerotic lesions, probably by inducing macrophage SR-AI mediated uptake.

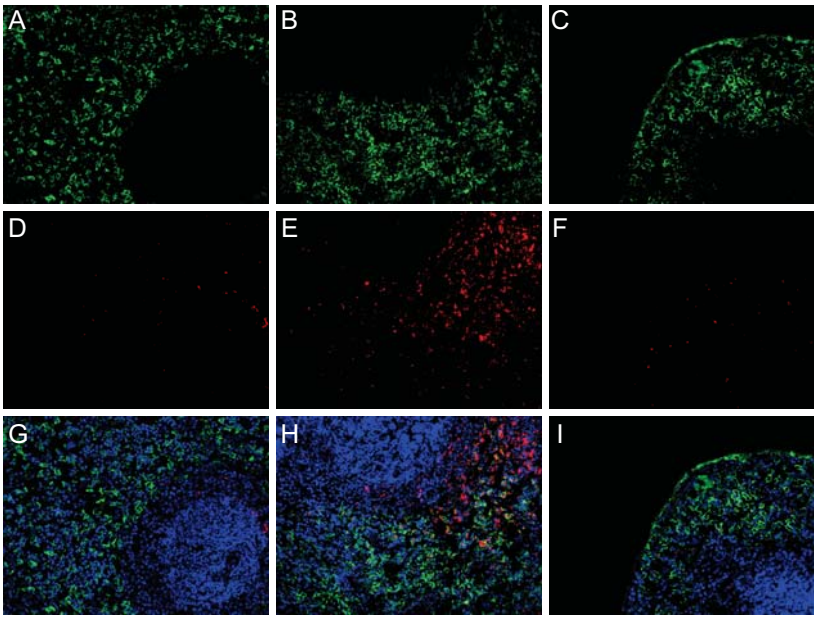

Figure 2.6 Streptavidin-PE docked PP1 colocalizes with splenic macrophages in a scavenger receptor dependent manner. Streptavidin PE conjugated PP1 was administered by tail vein injection to C57Bl/6 (B, E, H) or SR-A$^{-/-}$CD36$^{-/-}$ mice (C, F, I, n=2). Mice were sacrificed and organs were harvested 1h after injection. StrepPE-biotin injected to C57Bl/6 mouse was used as a control (A, D, G). Representative merged photomicrographs of splenic cryosections stained for the presence of mouse macrophages by F4/80 (green), PP1 conjugate uptake by PE fluorescence (red) and nuclei by DAPI (blue) were given respectively. Colocalization of macrophage with PP1 is yellow (Magnification 20x).

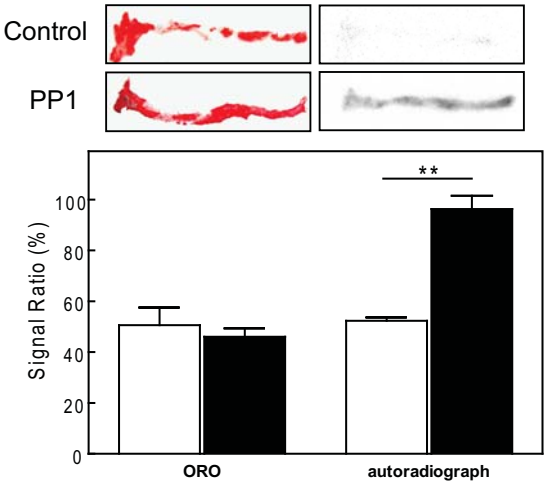

Figure 2.7 PP1 selectively targets atherosclerotic aortic lesions in ApoE$^{-/-}$ mice. ^{125}I strep-biotin or ^{125}I strep-bioPP1 (0.38 nmol/L) was intravenously injected into aged (>65 weeks) male ApoE$^{-/-}$ mice with advanced atherosclerosis (n=3). A representative Oil red O staining (upper left) and autoradiogram (upper right) of the aorta is shown. Relative lesion area (as a percentage of total aorta area; open bars) and the autoradiogram signal (as a percentage of the maximal signal in ^{125}I strep-BioPP1 treated group; black bars) are given in the lower panel (**: P<0.01).

DISCUSSION

Phage display of randomized peptides library has evolved into a very powerful strategy for the unbiased selection of peptide ligands that bind to diverse targets[25]. In search of potent and selective peptide antagonists for SR-AI we have employed phage display on a synthetic SR-AI receptor template. This synthetic SR-AI receptor contained part of the collagen-like SR-AI domain to allow trimerization of the peptide, and was earlier shown to adopt a configuration and ligand binding pattern that is very similar to that of SR-AI itself[8]. We argued that the use of synthetic SR-AI ligand binding domain rather than the complete receptor as selection template would bias the selection towards antagonists that interact with the actual binding pocket of SR-AI. Phage selection was successful and led to the identification of SR-AI specific phage clones, with a shared 11-mer consensus motif in their insert. The C-terminus of the two peptides differed, suggesting that in particular the N-terminal part is relevant to SR-AI binding, which is congruent with the fact that in the phage displayed peptide library peptides are fused at their C-terminal end to the coat protein (pIII). The peptide truncation studies revealed that deletion of up to four N-terminal amino acids was quite well tolerated in that the affinity of these truncated peptides for SR-AI was only slightly reduced. Actually, N-terminal biotinylated PP1 exhibited sharply reduced SR-AI binding after docking to streptavidin, confirming the importance of an exposed N-terminus. Together with the truncation studies these findings firmly establish the N-terminal part of the peptide as minimal essential motif for SR-AI binding.

The 15-mer linear peptide lead was capable of displacing phage binding to SR-AI at an IC_{50} of 29mmol/L (51.2µg/mL), which renders it only 5-fold less potent than poly-I (IC_{50}=10.5µg/mL), one of the most potent SR-AI inhibitors to date. SR-AI acts as a trimer and was shown to display a preference for oligomers[26]. We therefore argued that the affinity of PP1 for SR-AI may benefit from tetrameric presentation on a streptavidin scaffold[27], with the additional advantage that streptavidin docking may favourably affect its pharmacokinetics *in vivo*. We indeed observed that multimerization of PP1 resulted in an enhanced nanomolar potency for macrophage binding as shown in fucoidan displacement assay. Importantly, phage encoded peptides are also expressed as multimer on M13 phage. Ligand multimerization could in that sense emulate the peptide configuration on the phage coat protein.

The enriched phage appeared to be very specific for SR-AI as it did not bind to polystyrene, collagen or streptavidin immobilized biotin. Phage binding to SR-AI could be inhibited by established SR-AI inhibitors, suggesting that the phage clone indeed interacts with the collagen like ligand binding domain of SR-AI. The SR-AI binding phage not only bound avidly to the synthetic receptor but also to human THP-1 cells and, to a lesser extent, to murine RAW 264.7 cells, which both express high levels of SR-AI. The higher binding to THP-1 cells may be

attributable to interspecies differences as selection was based on bovine SR-AI, or to differences in SR-AI expression levels between the two cell lines as has previously been reported for P-selectin phage display[27]. Background binding of the selected phage to SR-AI deficient COS-7 cells was very low, which is a clear advantage when aiming at targeted delivery and imaging approaches *in vivo*. Streptavidin immobilized PP1 is internalized by macrophages in a SR-AI dependent fashion *in vitro*. The altered *in vivo* kinetics of PP1 *in vivo* in SR-AI$^{-/-}$ CD36 $^{-/-}$ mice concurs well with this notion. Together with the fact that CD36 does not bind to polyanionic ligands specific for SR-A such as poly-I while poly-I could displace specific phage binding to SR-AI[28], this indicates that immobilized PP1 uptake is solely SR-AI dependent.

Interestingly, protein BLAST search for short, nearly exact matches of PP1 revealed a high homology of the N-terminal heptapeptide LSLERFL to viruses such as human cytomegalovirus (CMV) and HIV (Supplement Tab. 1), which both have been implicated in atherosclerosis[29]. As SR-AI was found to interact with gram-positive bacteria[10], it is tempting to speculate that macrophage uptake of these pathogens may be at least partly SR-AI mediated and proceed through the LSLERFL motif. Further research will be required to establish the involvement of SR-AI in cellular uptake of these infectious agents.

Since macrophages play an important role in innate immunity and atherogenesis, SR-AI had been adopted as a favourable modality for macrophage targeting, for example, maleylated BSA, oxLDL and photosensitizer[30]. Previously we also developed a SR-A-specific particulate system for macrophage targeting which was based on an oligodeoxyguanosine ligand (dG_{10})[28]. However, the poor specificity and Toll like receptor dependent immune responses displayed by dG10 may disqualify it for widespread clinical use. The use of the described synthetic, selective antagonists with high affinity for SR-AI might overcome these pitfalls. Furthermore the low immunogenicity and higher penetration capacity may contrast favourably to that of macromolecular SR-AI ligands, that have until now been exploited for this purpose. SR-AI selective binding phage and streptavidin conjugated PP1 exhibited a similar biodistribution pattern *in vivo* with liver being the major site of elimination. In addition, the uptake pattern of PP1 is comparable to that of dG_{10} , indicating that liver macrophages account for the bulk of SR-A ligand clearance[28]. The higher phage accumulation in heart, spleen and lung as compared to that for the PP1/Streptavidin conjugate likely reflects intrinsic differences in M13 phage versus streptavidin clearance. It should be noted that the relative organ uptake of ^{125}I-streptavidin that is attributable to SR-AI may in fact be considerably underestimated due to the very effective breakdown and excretion of iodinated substrates by SR-AI.

The development of non-invasive molecular imaging modalities for assessment of rupture prone atherosclerotic lesions continues to be a major challenge. Most efforts, such as superparamagnetic iron oxide (SPIO/USPIO) particles for enhanced magnetic resonance imaging, are still based on their preferential passive

internalization by macrophages. In addition, potential immunomodulatory effects of SPIO/USPIO particles *in vivo* warrant further investigation. In contrast, receptor targeted uptake strategies as presented in this study for SR-AI could provide improved specificity while minimizing adverse side-effects. Unlike macromolecule ligands for SR-AI, the PP1 homing peptide offers the further advantage that it can be flexibly introduced into the imaging modality and synthesized in a chemically controlled manner.

In conclusion, a novel phage display strategy, based on biopanning on a synthetic template encompassing the binding domain of the target receptor, was successfully applied for the design of SR-AI peptide antagonists. Apart from its antagonistic capacity, the PP1 lead was able to target SR-AI expressing cells in vitro and *in vivo* after docking to a streptavidin scaffold. Moreover, we demonstrate that PP1 is able to redirect imaging modalities to atherosclerotic lesions *in vivo*. Given the preference of PP1 for human SR-AI, it is not unconceivable that the SR-AI and plaque homing capacity of this ligand in humans may even be superior to that in mice. This lead may thus not only form the promising starting point for the design of even more potent SR-AI inhibitors but also prove useful in the development of imaging and targeting strategies aimed at macrophage enriched sites of inflammation such as the atherosclerotic plaque.

REFERENCES

1. Ross R. Atherosclerosis--an inflammatory disease. *N Engl J Med* 1999;340:115-126.
2. Kodama T, Freeman M, Rohrer L, Zabrecky J, Matsudaira P, Krieger M. Type I macrophage scavenger receptor contains alpha-helical and collagen-like coiled coils. *Nature* 1990;343:531-535.
3. Penman M, Lux A, Freedman NJ, Rohrer L, Ekkel Y, McKinstry H, Resnick D, Krieger M. The type I and type II bovine scavenger receptors expressed in Chinese hamster ovary cells are trimeric proteins with collagenous triple helical domains comprising noncovalently associated monomers and Cys83-disulfide-linked dimers. *J Biol Chem* 1991;266:23985-23993.
4. Suzuki H, Kurihara Y, Takeya M, Kamada N, Kataoka M, Jishage K, Ueda O, Sakaguchi H, Higashi T, Suzuki T, Takashima Y, Kawabe Y, Cynshi O, Wada Y, Honda M, Kurihara H, Aburatani H, Doi T, Matsumoto A, Azuma S, Noda T, Toyoda Y, Itakura H, Yazaki Y, Kodama T, . A role for macrophage scavenger receptors in atherosclerosis and susceptibility to infection. *Nature* 1997;386:292-296.
5. Gough PJ, Greaves DR, Gordon S. A naturally occurring isoform of the human macrophage scavenger receptor (SR-A) gene generated by alternative splicing blocks modified LDL uptake. *J Lipid Res* 1998;39:531-543.
6. Rohrer L, Freeman M, Kodama T, Penman M, Krieger M. Coiled-coil fibrous domains mediate ligand binding by macrophage scavenger receptor type II. *Nature* 1990;343:570-572.
7. Doi T, Higashino K, Kurihara Y, Wada Y, Miyazaki T, Nakamura H, Uesugi S, Imanishi T, Kawabe Y, Itakura H, . Charged collagen structure mediates the recognition of negatively charged macromolecules by macrophage scavenger receptors. *J Biol Chem* 1993;268:2126-2133.
8. Tanaka T, Nishikawa A, Tanaka Y, Nakamura H, Kodama T, Imanishi T, Doi T. Synthetic collagen-like domain derived from the macrophage scavenger receptor binds acetylated low-density lipoprotein in vitro. *Protein Eng* 1996;9:307-313.
9. Nagelkerke JF, Barto KP, Van Berkel TJ. In vivo and in vitro uptake and degradation of acetylated low density lipoprotein by rat liver endothelial, Kupffer, and parenchymal cells. *J Biol Chem* 1983;258:12221-12227.
10. Dunne DW, Resnick D, Greenberg J, Krieger M, Joiner KA. The type I macrophage scavenger receptor binds to gram-positive bacteria and recognizes lipoteichoic acid. *Proc Natl Acad Sci U S A* 1994;91:1863-1867.
11. Van Berkel TJ, Van Velzen A, Kruijt JK, Suzuki H, Kodama T. Uptake and catabolism of modified LDL in scavenger-receptor class A type I/II knock-out mice. *Biochem J* 1998;331 (Pt 1):29-35.
12. Daugherty A, Cornicelli JA, Welch K, Sendobry SM, Rateri DL. Scavenger receptors are present on rabbit aortic endothelial cells in vivo. *Arterioscler Thromb Vasc Biol* 1997;17:2369-2375.
13. Pitas RE. Expression of the acetyl low density lipoprotein receptor by rabbit fibroblasts and smooth muscle cells. Up-regulation by phorbol esters. *J Biol Chem* 1990;265:12722-12727.
14. Gough PJ, Greaves DR, Suzuki H, Hakkinen T, Hiltunen MO, Turunen M, Herttuala SY, Kodama T, Gordon S. Analysis of macrophage scavenger receptor (SR-A) expression in human aortic atherosclerotic lesions. *Arterioscler Thromb Vasc Biol* 1999;19:461-471.
15. de Winther MP, van Dijk KW, Havekes LM, Hofker MH. Macrophage scavenger receptor class A: A multifunctional receptor in atherosclerosis. *Arterioscler Thromb Vasc Biol* 2000;20:290-297.
16. Babaev VR, Gleaves LA, Carter KJ, Suzuki H, Kodama T, Fazio S, Linton MF. Reduced atherosclerotic lesions in mice deficient for total or macrophage-specific expression of scavenger receptor-A. *Arterioscler Thromb Vasc Biol* 2000;20:2593-2599.
17. Li AC, Glass CK. The macrophage foam cell as a target for therapeutic intervention. *Nat Med* 2002;8:1235-1242.
18. Matsumoto A, Naito M, Itakura H, Ikemoto S, Asaoka H, Hayakawa I, Kanamori H, Aburatani H, Takaku F, Suzuki H, . Human macrophage scavenger receptors: primary structure, expression, and localization in atherosclerotic lesions. *Proc Natl Acad Sci U S A* 1990;87:9133-9137.
19. Lysko PG, Weinstock J, Webb CL, Brawner ME, Elshourbagy NA. Identification of a small-molecule, nonpeptide macrophage scavenger receptor antagonist. *J Pharmacol Exp Ther* 1999;289:1277-1285.
20. Suzuki K, Yamada T, Tanaka T. Role of the buried glutamate in the alpha-helical coiled coil domain of the macrophage scavenger receptor. *Biochemistry* 1999;38:1751-1756.

21. Molenaar TJ, Michon I, de Haas SA, Van Berkel TJ, Kuiper J, Biessen EA. Uptake and processing of modified bacteriophage M13 in mice: implications for phage display. *Virology* 2002;293:182-191.

22. Smookler DS, Mohammed FF, Kassiri Z, Duncan GS, Mak TW, Khokha R. Tissue inhibitor of metalloproteinase 3 regulates TNF-dependent systemic inflammation. *J Immunol* 2006;176:721-725.

23. Hughes DA, Fraser IP, Gordon S. Murine macrophage scavenger receptor: in vivo expression and function as receptor for macrophage adhesion in lymphoid and non-lymphoid organs. *Eur J Immunol* 1995;25:466-473.

24. Kunjathoor VV, Febbraio M, Podrez EA, Moore KJ, Andersson L, Koehn S, Rhee JS, Silverstein R, Hoff HF, Freeman MW. Scavenger receptors class A-I/II and CD36 are the principal receptors responsible for the uptake of modified low density lipoprotein leading to lipid loading in macrophages. *J Biol Chem* 2002;277:49982-49988.

25. Smith GP, Petrenko VA. Phage Display. *Chem Rev* 1997;97:391-410.

26. Pearson AM, Rich A, Krieger M. Polynucleotide binding to macrophage scavenger receptors depends on the formation of base-quartet-stabilized four-stranded helices. *J Biol Chem* 1993;268:3546-3554.

27. Molenaar TJ, Appeldoorn CC, de Haas SA, Michon IN, Bonnefoy A, Hoylaerts MF, Pannekoek H, Van Berkel TJ, Kuiper J, Biessen EA. Specific inhibition of P-selectin-mediated cell adhesion by phage display-derived peptide antagonists. *Blood* 2002;100:3570-3577.

28. Rensen PC, Gras JC, Lindfors EK, Van Dijk KW, Jukema JW, Van Berkel TJ, Biessen EA. Selective targeting of liposomes to macrophages using a ligand with high affinity for the macrophage scavenger receptor class A. *Curr Drug Discov Technol* 2006;3:135-144.

29. Ngeh J, Anand V, Gupta S. Chlamydia pneumoniae and atherosclerosis -- what we know and what we don't. *Clin Microbiol Infect* 2002;8:2-13.

30. de Vries HE, Moor AC, Dubbelman TM, Van Berkel TJ, Kuiper J. Oxidized low-density lipoprotein as a delivery system for photosensitizers: implications for photodynamic therapy of atherosclerosis. *J Pharmacol Exp Ther* 1999;289:528-534.